JOURNAL OF BACTERIOLOGY, Apr. 2007, p. 2618–2628 Vol. 189, No. 7
0021-9193/07/$08.00+0 doi:10.1128/JB.01905-06

Functional Characterization and Membrane Topology of *Escherichia coli* WecA, a Sugar-Phosphate Transferase Initiating the Biosynthesis of Enterobacterial Common Antigen and O-Antigen Lipopolysaccharide[▽]

Jason Lehrer,[1]† Karen A. Vigeant,[1]†‡ Laura D. Tatar,[1] and Miguel A. Valvano[1,2]*

Infectious Diseases Research Group, Siebens-Drake Medical Research Institute, Departments of Microbiology and Immunology[1] and Medicine,[2] University of Western Ontario, London, Ontario N6A 5C1, Canada

Received 18 December 2006/Accepted 15 January 2007

WecA is an integral membrane protein that initiates the biosynthesis of enterobacterial common antigen and O-antigen lipopolysaccharide (LPS) by catalyzing the transfer of *N*-acetylglucosamine (GlcNAc)-1-phosphate onto undecaprenyl phosphate (Und-P) to form Und-P-P-GlcNAc. WecA belongs to a large family of eukaryotic and prokaryotic prenyl sugar transferases. Conserved aspartic acids in putative cytoplasmic loops 2 (Asp90 and Asp91) and 3 (Asp156 and Asp159) were targeted for replacement mutagenesis with either glutamic acid or asparagine. We examined the ability of each mutant protein to complement O-antigen LPS synthesis in a *wecA*-deficient strain and also determined the steady-state kinetic parameters of the mutant proteins in an in vitro transfer assay. Apparent K_m and V_{max} values for UDP-GlcNAc, Mg^{2+}, and Mn^{2+} suggest that Asp156 is required for catalysis, while Asp91 appears to interact preferentially with Mg^{2+}, possibly playing a role in orienting the substrates. Topological analysis using the substituted cysteine accessibility method demonstrated the cytosolic location of Asp90, Asp91, and Asp156 and provided a more refined overall topological map of WecA. Also, we show that cells expressing a WecA derivative C terminally fused with the green fluorescent protein exhibited a punctate distribution of fluorescence on the bacterial surface, suggesting that WecA localizes to discrete regions in the bacterial plasma membrane.

Lipopolysaccharide (LPS), an abundant outer leaflet component of the gram-negative bacterial outer membrane, consists of three regions: lipid A, core oligosaccharide, and in some bacteria O-specific polysaccharide or O antigen (43, 52). O-antigen biosynthesis is a multistep process (43), which begins on the cytoplasmic face of the plasma membrane with the incorporation of carbohydrate components donated from nucleotide diphosphate sugar precursors. The *wb** cluster (formerly *rfb*) (44) encodes enzymes used for synthesis of nucleotide diphosphate sugars, specific glycosyltransferases, and membrane proteins for translocation of the O unit across the plasma membrane and formation of O-antigen polymers (43, 48, 52).

O antigens are polysaccharides consisting of repeating oligosaccharide units (O units). The biosynthesis of an O unit starts on the cytosolic face of the plasma membrane with the formation of a sugar phosphodiester linkage with undecaprenyl phosphate (Und-P). After the initiation reaction, additional sugars are incorporated to complete the O unit in reactions catalyzed by specific glycosyltransferases, which are either soluble cytosolic enzymes or peripheral membrane proteins associated with the plasma membrane by ionic interactions (43, 52, 56).

The initiation reaction is catalyzed by two different classes of integral membrane proteins (52). One class, the polyisoprenyl-phosphate *N*-acetylhexosamine-1-phosphate transferases (PNPTs), comprises proteins that are found in both prokaryotes and eukaryotes (14, 25, 42, 52). The prototype bacterial PNPT is WecA, a tunicamycin-sensitive UDP-*N*-acetylglucosamine (GlcNAc):Und-P GlcNAc-1-P transferase (37). WecA initiates O-unit synthesis in many *Escherichia coli* O types (1, 45, 58), *Klebsiella pneumoniae* O1 (11), *Shigella dysenteriae* (22), *Shigella flexneri* (58), and *Salmonella enterica* serovar Borreze (21), and it is also required for synthesis of the enterobacterial common antigen (38). Prokaryotic and eukaryotic PNPTs exhibit significant amino acid sequence similarity in certain regions of the protein (3, 4), underscoring the functional conservation of this class and presumably a common enzymatic mechanism (14, 28, 42, 52). Eukaryotic PNPTs are in the endoplasmic reticulum membrane, where they catalyze the transfer of GlcNAc-1-P to dolichol phosphate, the first step in N-linked glycoprotein biosynthesis (25). Bacterial members of this class, such as WecA, MraY, WbpL, and WbcO, can utilize different *N*-acetylhexosamine substrates, and they also differ in their susceptibilities to selective inhibitors (6, 42). The other class of prenyl sugar transferases includes the polyisoprenyl-phosphate hexose-1-phosphate transferases, and the prototype is WbaP (formerly RfbP) of *S. enterica*, in which the initiating sugar is galactose (54). The polyisoprenyl-phosphate hexose-1-phosphate transferases are unique to prokaryotes and are unrelated to PNTPs.

The WecA protein has not been purified to homogeneity. However, both biochemical information and genetic informa-

* Corresponding author. Mailing address: Department of Microbiology and Immunology, Dental Sciences Building 3014, University of Western Ontario, London, ON N6A 5C1, Canada. Phone: (519) 661-3427. Fax: (519) 661-3499. E-mail: mvalvano@uwo.ca.

† J.L. and K.A.V. contributed equally to this work.

‡ Present address: Bioniche Life Sciences Inc., Belleville, ON K8N 1E2, Canada.

▽ Published ahead of print on 19 January 2007.

tion support the hypothesis that its role involves the transfer of GlcNAc-1-P from UDP-GlcNAc to Und-P to form an Und-P-P-GlcNAc intermediate (37, 46). WecA can also transfer *N*-acetylgalactosamine-1-phosphate, as it is also essential for the synthesis of O antigens containing *N*-acetylgalactosamine (55). Furthermore, this enzyme has specificity for Und-P and cannot function with the eukaryotic lipid carrier dolichol phosphate (46). A predicted topological model for WecA suggests that there are 11 transmembrane segments, five cytosolic loops, and five periplasmic loops (5). We have previously identified highly conserved aspartic acids in two predicted cytosolic loops of WecA: Asp90 and Asp91 in cytosolic loop 2 and Asp156 and Asp159 in cytosolic loop 3 (4). Replacement of these residues with other amino acids affected the function of WecA, as demonstrated by the lack of in vitro enzymatic activity or reduced in vitro enzymatic activity of the mutated proteins, which could not mediate O-antigen LPS production in vivo (4). Aspartic acids have nucleophilic side chains, which may be involved in binding divalent metal ions (most commonly Mn^{2+} or Mg^{2+}) or in catalysis (23, 47, 59), as shown previously for other glycosyl and prenyl transferases (10, 33, 34, 50). We hypothesized that Asp90, Asp91, Asp156, and Asp159 are important for the catalytic activity of WecA (4). In this study, we characterized in more detail the functional roles of the conserved aspartic acids of WecA. Together, the in vivo activities of parental WecA and mutated WecA (having conservative amino acid replacements) and the steady-state kinetic parameters of these proteins demonstrated that Asp90/Asp91 and Asp156/Asp159 define two distinct functional regions in the protein. A refined topological map of WecA, based on the substituted cysteine accessibility method (8), conclusively demonstrated that Asp90/Asp91 and Asp156/Asp159, as well a critical histidine in the predicted cytosolic loop 5, His278 (3), are exposed to the cytosolic side of the plasma membrane. We also found that the C terminus of WecA is exposed to the cytosol and provide evidence suggesting that WecA localizes in discrete regions of the bacterial membrane.

MATERIALS AND METHODS

Strains and growth conditions. The properties of the *E. coli* strains used in this study are described in Table 1. Strain MV501, a *wecA*::Tn*10* mutant (1), was used to assess protein expression of all constructs and for in vivo complementation studies. *E. coli* DH5α was used for plasmid maintenance and recovery after mutagenesis. Bacteria were cultured at 37°C in Luria-Bertani (LB) medium supplemented with ampicillin (100 μg/ml), tetracycline (20 μg/ml), and 0.2% (wt/vol) arabinose, when appropriate. Transformation was performed by either the calcium chloride method or electroporation, as described elsewhere (12, 15). All biochemical reagents were purchased from Sigma (St. Louis, MO), unless indicated otherwise. Restriction endonucleases, T4 DNA ligase, and associated buffers were purchased from Roche Molecular Biochemicals (Dorval, Quebec, Canada).

PCR and cloning strategies. PCRs were carried out with a PTC-200 Peltier thermal cycler (MJ Research Inc, Watertown, MA). The plasmid containing the $wecA_{FLAG\text{-}5\times His}$ gene was constructed by amplification of a 1.2-kb fragment using pAA26 as the template (5) and the sense and antisense primers 5′-GCG ACACATATGAATTTACTGACAGTGAGT-3′ (NdeI site underlined) and 5′-GGTCGGAGCTCTTGTCGTCGTCGTCCTTGTAGTCTTC-3′ (SacI site underlined), respectively. The amplicon was digested with NdeI and SacI and ligated to NdeI-SacI ends of pBAD-His (Table 1). This plasmid is a modified pBAD24 plasmid (17) that contains an oligonucleotide sequence encoding a six-His oligopeptide, which was placed adjacent to the multiple cloning site for construction of C-terminally His-tagged fused proteins. The resulting plasmid, designated pKV1, expressed a five-His-tagged form of the $WecA_{FLAG}$ protein under control of the arabinose-inducible promoter, as one of the His residues was lost during construction. Site-directed mutagenesis was conducted with a QuikChange kit from Stratagene (La Jolla, CA) using pKV1 as the template DNA, as specified by the supplier. The mutagenic oligonucleotide primers contained nucleotide replacements modifying the original codons of the targeted amino acids. The sequences of these primers and the PCR amplification conditions are available upon request. Plasmid pKV1 was used as a template to replace all native cysteine residues of WecA (residues 60, 79, 167, 189, and 337) with alanine by sequential site-directed mutagenesis. The plasmid encoding the cysteineless $WecA_{FLAG\text{-}5\times His}$ protein was designated pJL5. This plasmid was further modified by mutagenesis to express cysteineless $WecA_{FLAG\text{-}7\times His}$, resulting in pJL7. Plasmid pLDT29 encoding WecA C terminally fused to the green fluorescent protein (GFP) was constructed by amplifying the promoterless *gfpmut3* gene from pFV25 (51) with primers having PstI ends. This amplicon was ligated into pAA26 encoding $wecA_{FLAG}$ (5), also digested with PstI, resulting in replacement of the DNA sequence encoding the FLAG epitope by the *gfpmut3* gene. All constructs were verified by DNA sequencing, which was carried out at the DNA Sequencing Facility, Robarts Research Institute (London, Ontario, Canada).

TABLE 1. Characteristics of the bacterial strains and plasmids used in this study

Strain or plasmid	Relevant properties[a]	Reference or source
E. coli strains		
CLM37	W3110 Δ*wecA*	26
DH5α	*E. coli* K-12 F^- ϕ80*lacZ*ΔM15 *endA recA hsdR*(r_K^- m_K^-) *supE thi gyrA relA* Δ(*lacZYA-argF*)*U169*	Laboratory stock
MV501	VW187; *wecA*::Tn*10* Tc^r	1
VW187	O7:K1; clinical isolate	53
W3110	*E. coli* K-12 *rph-1* IN(*rrnD-rrnE*)*1*	Laboratory stock
Plasmids		
pAA26	1.2-kb EcoRI-PvuII fragment from pAA14 containing $wecA_{FLAG}$ ligated into EcoRI and SmaI sites of pBAD24, Amp^r	5
pBAD-His	His_6 inserted into pBAD24, Amp^r	17; this study
pFV25	Plasmid encoding *gfpmut3*	51
pJL5	pKV1 expressing cysteineless $WecA_{FLAG\text{-}5\times His}$	This study
pJL7	pJL5 expressing cysteineless $WecA_{FLAG\text{-}7\times His}$	This study
pKV1	pAA26 expressing $WecA_{FLAG}$ tagged with His_5 ($WecA_{FLAG\text{-}5\times His}$), Amp^r	This study
pKV2	pKV1 expressing WecA-D90E$_{FLAG\text{-}5\times His}$	This study
pKV3	pKV1 expressing WecA-D90N$_{FLAG\text{-}5\times His}$	This study
pKV4	pKV1 expressing WecA-D91E$_{FLAG\text{-}5\times His}$	This study
pKV5	pKV1 expressing WecA-D91N$_{FLAG\text{-}5\times His}$	This study
pKV8	pKV1 expressing WecA-D156E$_{FLAG\text{-}5\times His}$	This study
pKV9	pKV1 expressing WecA-D156N$_{FLAG\text{-}5\times His}$	This study
pKV10	pKV1 expressing WecA-D159E$_{FLAG\text{-}5\times His}$	This study
pKV11	pKV1 expressing WecA-D159N$_{FLAG\text{-}5\times His}$	This study
pLDT29	pAA26 expressing $WecA_{GFP}$	This study

[a] Tc^r, tetracycline resistance; Amp^r, ampicillin resistance.

Membrane preparation. Bacterial cultures were grown overnight in 5 ml of LB medium, diluted to obtain an initial optical density at 600 nm (OD_{600}) of 0.02, and incubated at 37°C for 2 h until the OD_{600} was 0.5. At this point, arabinose was added to a final concentration of 0.2%, and cells were incubated for an additional 2 h until the OD_{600} was between 0.8 and 1.0. Cells were then harvested by centrifugation at 10,000 × *g* for 10 min at 4°C, and each resulting pellet was washed, resuspended in 0.9% (vol/vol) NaCl, and centrifuged again as described above. The bacterial pellet was suspended in 50 mM Tris acetate (pH 8.5), and the suspension was lysed using a French press. Insoluble debris was removed by centrifugation (15,000 × *g* for 15 min at 4°C), and the clear supernatant was centrifuged at 30,000 × *g* for 25 min at 4°C. The pellet, containing total membranes, was suspended in 40 mM Tris acetate (pH 8.5) and frozen at −80°C until it was used.

LPS analysis. LPS was extracted as described previously (32). Briefly, cells from overnight plate cultures were suspended in a lysis buffer containing proteinase K, which was followed by hot phenol extraction and subsequent extraction of the aqueous phase with ether. LPS was resolved by electrophoresis in 14% polyacrylamide gels using a Tricine-sodium dodecyl sulfate (SDS) system and

was visualized by silver staining (30). The concentration of LPS was determined by the keto-deoxyoctulosonic (KDO) assay (40).

Transferase assay and kinetic analysis. The reaction mixture used for the standard in vitro transferase assay (modified from the mixture used by McGrath and Osborn [35]) contained 40 μg total protein membrane fraction (providing the enzyme and the endogenous Und-P acceptor), 0.2 mM $MnCl_2$ or 1 mM $MgCl_2$, and 131.4 pmol of radiolabeled UDP-*N*-acetyl-[^{14}C]glucosamine (225 mCi/mmol) in 250 μl of buffer (5 mM Tris acetate [pH 8.5]). After incubation at 37°C for 15 min, the lipid-associated material was extracted twice with 150 μl of 1-butanol. The combined 1-butanol extracts were washed once with 300 μl of distilled water. The radioactive count for a 150-μl aliquot of the 1-butanol fraction was determined with a Beckman liquid scintillation counter (Beckman Coulter Canada Inc., Mississauga, Ontario, Canada). Radioactive counts were normalized for the background value. To determine the divalent metal ion requirements, incorporation of UDP-GlcNAc into the lipid fraction was established using various concentrations of Mg^{2+} and Mn^{2+} (0 to 3 mM) with a fixed amount of UDP-GlcNAc (131.4 pmol). The kinetic parameters for UDP-GlcNAc were determined with excess Mg^{2+} or Mn^{2+} and amounts of UDP-GlcNAc ranging from 8.76 to 175.2 pmol. Data were analyzed by nonlinear regression using GraphPad Prism v.4 and the Michaelis-Menten equation. One unit of enzyme activity was defined as 10^{-3} pmol GlcNAc incorporated into the lipid fraction per min per mg of total protein. In some experiments, product conversion was examined by thin-layer chromatography (TLC). To do this, 200 μl of the 1-butanol fraction was dried in a microcentrifuge tube and resuspended in 20 μl chloroform-methanol (2:1), and 4-μl portions were spotted onto a Whatman silica gel (PE SIL G) plate, which was developed in a solvent containing di-isobutylketone, acetic acid, and water (80:50:10), as described previously (19). After drying and overnight exposure of the plate to a PhosphorImager screen, product formation was detected and quantified with a PhosphorImager (Storm 840; Amersham Biosciences) equipped with Image-Quant software. Purified Und-P and Und-P-P were obtained from the Institute of Biochemistry and Biophysics, Polish Academy of Sciences, Warsaw, Poland.

Preparation of cells and vesicles for labeling with sulfhydryl-reactive reagents. LB medium (500 ml) supplemented with 100 μg/ml ampicillin and 20 μg/ml tetracycline was inoculated with an overnight culture of strain MV501 cells containing the appropriate plasmids. The cells were grown and protein expression was induced with arabinose as described above. At the end of the induction period the culture was split into two 250-ml aliquots for orientation-specific labeling. Bacteria were harvested by centrifugation at 3,300 × *g* for 15 min, washed twice with 0.1 M sodium phosphate buffer (pH 7.5), and resuspended in 25 ml of buffer. One aliquot was pretreated with 0.5 mM [2-(trimethylammonium)ethyl] methanethiosulfonate bromide (MTSET) (Toronto Research Chemicals Inc., Toronto, Ontario, Canada) for 10 min at room temperature. Both aliquots were then treated with 0.5 mM N^{α}-(3-maleimidylpropionyl)biocytin (biotin maleimide) (Molecular Probes, Portland, OR) for 10 min at room temperature, with occasional shaking. The reaction was terminated by addition of 500 μl of 2% (vol/vol) 2-mercaptoethanol in 0.1 M sodium phosphate buffer. Treated cultures were then washed twice with 20 ml phosphate buffer and lysed with two treatments at 15,000 lb/in^2 using a French press. The lysates were centrifuged at 39,000 × *g* for 15 min, and each supernatant was pelleted by centrifugation at 280,000 × *g* for 30 min. The pellet, containing total membranes, was resuspended in 1 ml of 0.1 M sodium phosphate buffer, and 50 μl was solubilized with 0.5% Triton X-100 in 0.1 M sodium phosphate buffer with 8 M urea (pH 7.8) for 2 h.

Purification of His-tagged protein. Solubilized samples were centrifuged at 39,000 × *g* for 15 min to remove insoluble material. One hundred microliters of cobalt-bound chelating Sepharose Fast Flow resin (GE Healthcare), equilibrated with wash buffer (0.1 M sodium phosphate, 300 mM NaCl, 100 mM imidazole, 8 M urea; pH 7.8) was mixed with the supernatant in a microcentrifuge tube. After 1 h of gentle mixing at room temperature, the resin was centrifuged at 1,000 × *g* for 1 min, the supernatant was aspirated, and the protein-loaded column was washed three times with 1 ml of wash buffer. WecA was eluted by incubating the resin with 100 μl of elution buffer (0.1 M sodium phosphate, 300 mM NaCl, 300 mM imidazole, 8 M urea, 0.5% Triton X-100; pH 7.8) for 15 min.

Gel electrophoresis and analysis. Sodium dodecyl sulfate-polyacrylamide gel electrophoresis (PAGE), protein transfer to nitrocellulose membranes, and immunoblotting with the FLAG M2 monoclonal antibody were performed as described previously (4), except that the reacting bands were detected by fluorescence with an Odyssey infrared imaging system (Li-cor Biosciences, Lincoln, NE) using Alexa Fluor 680 goat anti-mouse secondary antibody (Rockland Immunochemicals, Gilbertsville, PA). Various amounts (0.8 to 3.2 ng) of C-terminally FLAG-tagged bacterial alkaline phosphatase (BAP-FLAG) were loaded on the same gels as standards for quantitative immunoblotting (41). The pixel density of the gel bands was analyzed with ImageJ software (W. S. Rasband, U.S. National Institutes of Health, Bethesda, MD; http://rsb.info.nih.gov/ij/). Biotinylated proteins were detected by incubation with horseradish peroxidase-linked streptavidin and chemiluminescence using the BM chemiluminescence blotting substrate (Roche Diagnostics), as recommended by the manufacturer.

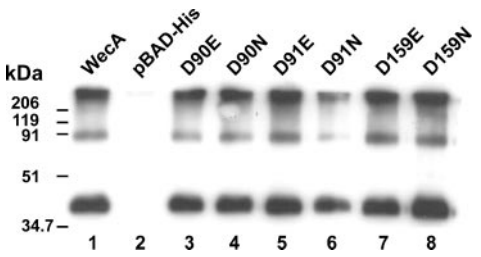

FIG. 1. Expression of parental WecA and mutant protein derivatives. Total membranes were prepared from strain MV501 (VW187 *wecA*::Tn*10*) transformed with various plasmids containing several versions of *wecA* (Table 1), as follows: lane 1, WecA(pKV1) ($wecA_{FLAG\text{-}5\times His}$); lane 2, pBAD-His vector control; lane 3, D90E protein, pKV2; lane 4, D90N protein, pKV3; lane 5, D91E protein, pKV4; lane 6, D91N protein, pKV5; lane 7, D159E protein, pKV10; lane 8, D159N protein, pKV11. Each lane contained 4 μg of protein. Membranes were transferred to a nitrocellulose membrane and reacted with anti-FLAG monoclonal antibodies. The molecular mass standards were myosin (206 kDa), β-galactosidase (119 kDa), bovine serum albumin (91 kDa), ovalbumin (51 kDa), and carbonic anhydrase (34.7 kDa).

Microscopy. An overnight culture of *E. coli* DH5α cells containing pLDT29, which expresses $WecA_{GFP}$ under control of the arabinose-inducible P_{BAD} promoter (Table 1), was diluted in LB medium to obtain an OD_{600} of 0.1, and protein expression was induced with arabinose as described above. After 3 h of induction, the culture was placed on ice for 1 to 2 h to facilitate GFP folding. Similar experiments were performed without arabinose in the growth medium. Bacteria were visualized with no fixation using an Axioscope 2 (Carl Zeiss) microscope with an ×100/1.3 numerical aperture Plan-Neofluor objective and a 50-W mercury arc lamp with a GFP band pass emission filter set (Chroma Technology) with excitation at 470 ± 20 nm and emission at 525 ± 25 nm. Images were digitally processed using the Northern Eclipse imaging analysis software (version 6.0; Empix Imaging, Mississauga, Ontario, Canada).

RESULTS

Functional characterization of $WecA_{FLAG\text{-}5\times His}$. Plasmid pKV1, encoding $WecA_{FLAG\text{-}5\times His}$, was constructed to provide WecA with the FLAG epitope tag for immunodetection and a C-terminal five-His sequence for purification by Ni^{2+} affinity chromatography. Plasmid pKV1 was transformed into *E. coli* MV501 (*wecA*::Tn*10*), and membranes isolated from the transformant were analyzed by SDS-PAGE and Western blotting. A 38-kDa polypeptide band (Fig. 1, lane 1), absent in membranes from the MV501(pBAD-His) control (Fig. 1, lane 2), was found in membranes from MV501(pKV1). The observed molecular mass for $WecA_{FLAG\text{-}5\times His}$ was lower than the predicted mass deduced from its amino acid sequence (44.8 kDa). The anomalous migration of WecA in SDS-PAGE was reported previously (3–5) and was probably due to the hydrophobicity and high pI of this protein (theoretical pI, 10.01) (20). The bands at higher molecular masses in the blot were likely due to $WecA_{FLAG\text{-}5\times His}$ oligomers that resulted from the mild denaturation conditions (incubation at 45°C for 30 min in loading sample buffer containing 50 mM Tris-HCl [pH 6.8], 2% SDS, 10% glycerol, and 0.1% bromophenol blue) used to visualize WecA since, as we previously reported (5), incubation at

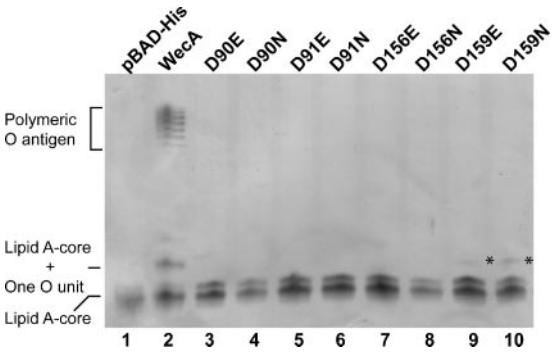

FIG. 2. Complementation of O7 LPS synthesis in strain MV501 (VW187 *wecA*::Tn*10*) by parental WecA and mutant derivatives. LPS samples were obtained from *E. coli* MV501 (VW187 *wecA*::Tn*10*) transformed with various plasmids. Lane 1, pBAD-His; lane 2, WecA(pKV1) ($wecA_{FLAG\text{-}5\times His}$); lane 3, D90E protein, pKV2; lane 4, D90N protein, pKV3; lane 5, D91E protein, pKV4; 6 lane, D91N protein, pKV5; lane 7, D156E protein, pKV8; lane 8, D156N protein, pKV9; lane 9, D159E protein, pKV10; lane 10, D159N protein, pKV11. LPS was separated by Tricine-SDS-PAGE, which was followed by silver staining. Loading was normalized by determining the amount of KDO in the inner core.

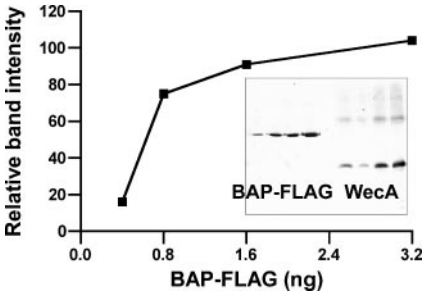

FIG. 4. Quantitative immunoblotting to determine the amounts of WecA in total membrane preparations. The relative amounts of FLAG molecules in the samples were determined by comparison with known amounts (0.4 to 3.2 ng) of purified BAP-FLAG, which were included on the same gel. The graph is a plot of the relative pixel densities of the BAP-FLAG bands, which were calculated with the program ImageJ, versus the amounts of purified protein loaded in the lanes. The inset shows the blot with the different amounts of BAP-FLAG (left four lanes) and $WecA_{FLAG\text{-}5\times His}$ (right four lanes). The amount of $WecA_{FLAG\text{-}5\times His}$ was deduced from the standard curve.

higher temperatures resulted in a failure to detect WecA. Plasmid pKV1 was sufficient to complement O7 LPS production in MV501 (Fig. 2, lane 2), demonstrating that $WecA_{FLAG\text{-}5\times His}$ was functional in vivo. Therefore, we concluded that the incorporation of two epitope tags in tandem into the C terminus of WecA resulted in a protein that not only can be targeted to the plasma membrane but also retains functionality compared with untagged WecA.

We next investigated the enzymatic activity of $WecA_{FLAG\text{-}5\times His}$. The product of the reaction, Und-P-P-GlcNAc, was directly identified using TLC plates. For this experiment, membranes were prepared from *E. coli* K-12 strain CLM37 (Δ*wecA*) carrying pKV1, and the lipid fraction containing the Und-P-P-GlcNAc product was extracted with 1-butanol. The radiolabeled control, UDP-GlcNAc, did not migrate beyond the loading point (R_f, 0.008) (Fig. 3, lane 1), but a spot with an R_f of 0.167 was detected in the extract from membranes containing $WecA_{FLAG\text{-}5\times His}$ (Fig. 3, lane 6). In the same buffer system, authentic Und-P and Und-P-P had R_f values of 0.64 and 0.38, respectively (data not shown). Based on these results, we deduced that the spot with an R_f of 0.167 corresponded to Und-P-P-GlcNAc. The kinetic parameters of the transfer of radiolabeled GlcNAc-1-P to Und-P were also determined. Membranes from MV501(pKV1), providing both the enzyme and the endogenous Und-P acceptor, were incubated with radioactive UDP-GlcNAc. The lipid fraction containing the Und-P-P-GlcNAc product was extracted with 1-butanol, and the radioactive counts in the 1-butanol extract reflected the amount of radiolabeled GlcNAc-1-P incorporated into Und-P. Under the standard conditions for this assay (1 mM Mg^{2+} and 40 μg of membrane proteins), we detected a level of product conversion of 120 nmol of GlcNAc incorporated into the lipid phase per mg of total membrane protein, corresponding to 8.8 U of enzyme activity. In addition, we estimated the amount of WecA in the membrane fractions by quantitative immunoblotting, using a similar strategy described previously (41). The total amount of WecA in the samples was determined by using C-terminal BAP-FLAG as a standard. An example of this analysis is shown in Fig. 4. The relative intensities of the bands were determined with the program ImageJ and were used to calculate the amount of $WecA_{FLAG\text{-}5\times His}$ in the membrane preparations, which corresponded to 27.5 ng of BAP-FLAG equivalents per 40 μg of membranes. Under these conditions, the in vitro incorporation profile was also linear as a function of time (data not shown).

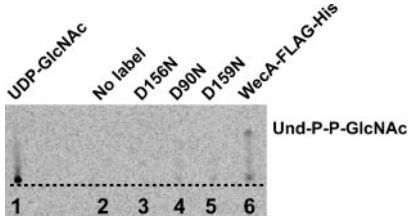

FIG. 3. Detection of Und-P-P-GlcNAc product conversion by thin-layer chromatography. Membranes of *E. coli* CLM37 harboring various plasmids were assayed for transferase activity under standard conditions with ^{14}C-labeled UDP-GlcNAc, and the lipid-linked material was extracted with 1-butanol and processed as described in Materials and Methods. Lane 1, ^{14}C-labeled UDP-GlcNAc, no membranes; lane 2, membranes from plasmidless CLM37, no ^{14}C-labeled UDP-GlcNAc; lane 3, membranes from CLM37(pVK9) expressing WecA-$D156N_{FLAG\text{-}5\times His}$; lane 4, membranes from CLM37(pVK3) expressing WecA-$D90N_{FLAG\text{-}5\times His}$; lane 5, membranes from CLM37(pVK11) expressing WecA-$D159N_{FLAG\text{-}5\times His}$; lane 6, membranes from CLM37(pVK1) expressing $WecA_{FLAG\text{-}5\times His}$. The dotted line indicates the loading point.

The transferase assay allowed us to determine the steady-state kinetics of enzyme activity in membranes containing $WecA_{FLAG\text{-}5\times His}$ using various UDP-GlcNAc concentrations in the presence of a 10-fold excess of Mg^{2+} (17 mM) or Mn^{2+} (3 mM). These metal ion concentrations represented 10-fold excesses relative to the K_m values calculated with Mg^{2+} and Mn^{2+} (see below). Similar curves were observed for the two metal ions (Fig. 5A). The apparent K_m values for UDP-GlcNAc were 0.12 ± 0.06 and 0.19 ± 0.05 μM in the presence

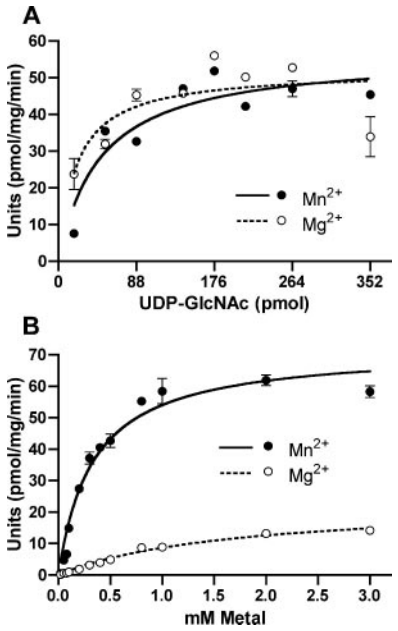

FIG. 5. Transfer of GlcNAc-1-P to Und-P. All assays were carried out at 37°C for 15 min in triplicate. One unit of enzyme activity was defined as 10^{-3} pmol of GlcNAc incorporated/min/mg protein. (A) UDP-GlcNAc-dependent activity of $WecA_{FLAG\text{-}5\times His}$ in the presence of excess Mg^{2+} (16.7 mM) and Mn^{2+} (3.1 mM). (B) Mg^{2+}- and Mn^{2+}-dependent enzyme activity of $WecA_{FLAG\text{-}5\times His}$. Assays were carried out at 37°C for 15 min with a fixed concentration of UDP-GlcNAc (131.4 pmol), 40 μg of total membranes from an MV501(pKV1) preparation, and different concentrations (0 to 3 mM) of Mg^{2+} and Mn^{2+}.

of Mg^{2+} and Mn^{2+}, respectively, while the V_{max} values were 57 ± 4 and 56.4 ± 3.5 pmol min^{-1}, respectively (Table 2 and data not shown). We investigated in more detail the metal ion requirements for $WecA_{FLAG\text{-}5\times His}$ enzyme activity. No transfer activity was detected in membranes incubated with Ca^{2+}, Co^{2+}, Ni^{2+}, Zn^{2+}, or 1 mM EDTA (data not shown), while either Mn^{2+} or Mg^{2+} activated the enzyme (Fig. 5B). In the presence of excess UDP-GlcNAc, the apparent K_m and V_{max} values with Mg^{2+} were 1.7 ± 0.2 mM and 23 ± 1.3 pmol min^{-1}, respectively, whereas the apparent K_m and V_{max} values with Mn^{2+} were 0.3 ± 0.04 mM and 71.7 ± 2.6 pmol min^{-1}, respectively (Table 3). These results indicate that in vitro and in the presence of excess UDP-GlcNAc, the enzyme is nearly six times more effective with Mn^{2+} than with Mg^{2+}.

Functional characterization of aspartic acids in predicted cytosolic loops 2 and 3 of $WecA_{FLAG\text{-}5\times His}$. To investigate the function of the highly conserved aspartic acids in predicted cytosolic loops 2 (Asp90 and Asp91) and 3 (Asp156 and Asp159), we constructed derivatives of $WecA_{FLAG\text{-}5\times His}$ with conservative amino acid replacements. In all cases, we generated two derivatives for each position by replacing the aspartic acid with either asparagine or glutamic acid. To rule out the possibility that the amino acid replacements compromised either protein stability or targeting to the plasma membrane, the expression of the $WecA_{FLAG\text{-}5\times His}$ mutant forms was investigated by Western blot analysis using MV501 membranes transformed with plasmids containing the mutated $wecA_{FLAG\text{-}5\times His}$ genes. All mutants with mutations in predicted cytosolic loops 2 and 3 had the same levels of expression as the parental $WecA_{FLAG\text{-}5\times His}$ strain (Fig. 1, lanes 3 to 8, and data not shown), and these results were also consistent with the similar amounts of $WecA_{FLAG\text{-}5\times His}$ and mutant forms in the membrane fractions, as estimated by quantitative immunoblotting.

Kinetic analyses, as described above for the parental $WecA_{FLAG\text{-}5\times His}$ protein, were performed to characterize in more detail the functional defects of each mutant protein. Membranes containing WecA-D156$E_{FLAG\text{-}5\times His}$ and WecA-D156$N_{FLAG\text{-}5\times His}$ did not exhibit any detectable transfer activity (Table 2) and, as expected, did not restore production of O7 antigen in strain MV501 (Fig. 2, lanes 7 and 8). Also, product conversion was not detected by TLC (Fig. 3, lane 3, and data not shown). These results suggest that Asp156 could be required for catalysis, by acting as a nucleophile for cleavage of the pyrophosphate bond of the biphosphate nucleotide sugar substrate. The GlcNAc-1-P transfer activity of membranes containing the D159E and D159N proteins was detectable but drastically reduced. In both cases, the enzyme exhibited a 10-fold increase in the apparent K_m for UDP-GlcNAc compared to the wild type and 1% relative efficiency (Table 2). These findings are consistent with the TLC results showing that product conversion in reactions with membranes containing WecA-D159$N_{FLAG\text{-}5\times His}$ was barely detectable, with less than 20% of the amount of Und-P-P-GlcNAc detected for parental $WecA_{FLAG\text{-}5\times His}$ (Fig. 3, lane 5). WecA-D159$E_{FLAG\text{-}5\times His}$ and WecA-D159$N_{FLAG\text{-}5\times His}$ mediated the production of small amounts of one O7 unit attached to the lipid A core (Fig. 2, lanes 9 and 10), confirming that the enzymes were poorly functional in vivo. The kinetic parameters for the Mg^{2+} and Mn^{2+} cofactors showed that there were small increases (≤2-fold compared to the values for the parental protein) in the apparent K_m values with both metals for WecA-D159$E_{FLAG\text{-}5\times His}$ and virtually no change for WecA-D159$N_{FLAG\text{-}5\times His}$. However, the small variations in K_m were associated with drastic reductions (range, 7- to 35-fold) in the V_{max} values (Table 3). The ratios of the K_m values for the proteins with Asp-to-Asn replacements to the

TABLE 2. Comparison of kinetic parameters of UDP-GlcNAc for parental and mutant $WecA_{FLAG\text{-}5\times His}$

Parental or mutant $WecA_{FLAG\text{-}5\times His}$ plasmid (protein form)	V_{max} (pmol/min/mg)[a]	K_m (μM)	Relative V_{max}/K_m
pKV1	56.4 ± 3.5	0.19 ± 0.05	100 (297)[b]
pKV2 (D90E)	23.6 ± 2.3	0.18 ± 0.07	43 (129)
pKV3 (D90N)	15.5 ± 2.0	0.12 ± 0.09	44 (130)
pKV4 (D91E)	32.7 ± 2.0	0.03 ± 0.02	392 (1,167)
pKV5 (D91N)	42.4 ± 3.8	0.17 ± 0.06	81 (242)
pKV8 (D156E)	ND	ND	NA
pKV9 (D156N)	ND	ND	NA
pKV10 (D159E)	5.9 ± 3.1	1.97 ± 1.55	1.0 (3)
pKV11 (D159N)	6.0 ± 3.3	1.84 ± 1.53	1.0 (3)

[a] Standard $WecA_{FLAG\text{-}His}$ assays were performed with total membrane extracts prepared from MV501 *E. coli* cells carrying the plasmids containing parental or mutant *wecA* genes with 10 times the concentration corresponding to the experimentally determined K_m for Mn^{2+}, as described in Materials and Methods. ND, no detectable activity above the background; NA, not applicable.

[b] The numbers in parentheses are the absolute values of dividing V_{max} by K_m.

TABLE 3. Comparison of kinetic parameters of Mn^{2+} and Mg^{2+} for parental and mutant $WecA_{FLAG\text{-}5\times His}$[a]

Parental or mutant $WecA_{FLAG\text{-}His}$	Mg^{2+}			Mn^{2+}		
	V_{max} (pmol/min/mg)	K_m (mM)	K_m(N)/K_m(E) ratio	V_{max} (pmol/min/mg)	K_m (mM)	K_m(N)/K_m(E) ratio
$WecA_{FLAG\text{-}His}$	23.0 ± 1.3	1.7 ± 0.2	NA	71.7 ± 2.6	0.3 ± 0.04	NA
D90E	21.3 ± 7	9.3 ± 3.8		22.3 ± 7.8	1.6 ± 0.8	
D90N	169.7 ± 43	11.0 ± 3.4	1.2	77.8 ± 14.3	0.94 ± 0.3	0.6
D91E	0.6 ± 0.2	0.5 ± 0.3		0.7 ± 0.1	0.08 ± 0.1	
D91N	39.4 ± 7	5.7 ± 1.4	11.4	44.3 ± 7	0.5 ± 0.1	6.2
D159E	3.1 ± 0.4	2.7 ± 0.6		2.3 ± 0.3	0.6 ± 0.2	
D159N	0.9 ± 0.4	1.4 ± 1.5	0.5	2.0 ± 0.4	0.3 ± 0.2	0.5

[a] Standard $WecA_{FLAG\text{-}His}$ assays were performed with total membrane extracts prepared from *E. coli* MV501 cells carrying plasmids containing parental or mutant *wecA* genes. The assays were performed as described in Materials and Methods. K_m(N), K_m for the protein with an asparagine substitution; K_m(E), K_m for the protein with a glutamic acid substitution; NA, not applicable.

K_m values for the proteins with the Asp-to-Glu replacements were used to estimate the relative affinities of the enzymes for metal ions. A ratio greater than 1 suggested that an enzyme had more affinity for a metal ion, while a ratio that was equal to or less than 1 indicated that the enzyme affinity for a metal ion did not vary despite the residue charge. The ratio of the K_m values for the D159N and D159E proteins was 0.5 with Mg^{2+} and Mn^{2+} (Table 3), suggesting that Asp159 does not interact with the metal ions. Collectively, the combined results of these experiments indicate that Asp156 and Asp159 are part of a putative catalytic center involved in binding or modification of the UDP-GlcNAc substrate.

The kinetic parameters for the GlcNAc-1-P transfer reactions with excess metal ion cofactors in membranes containing WecA-D90E$_{FLAG\text{-}5\times His}$, WecA-D90N$_{FLAG\text{-}5\times His}$, and WecA-D91N$_{FLAG\text{-}5\times His}$ revealed slightly reduced velocities and small increases in the apparent K_m for UDP-GlcNAc (Table 2). The data suggest that Asp90 and Asp91 do not directly interact with UDP-GlcNAc. Membranes containing WecA-D91E$_{FLAG\text{-}5\times His}$ exhibited a sixfold decrease in the apparent K_m for UDP-GlcNAc compared to the apparent K_m of the parental enzyme. However, despite the apparently higher enzymatic efficiency of WecA-D91E$_{FLAG\text{-}5\times His}$, none of the replacements at the Asp90 and Asp91 positions resulted in functional proteins, as determined by complementation of the WecA function in strain MV501 (Fig. 2, lanes 3 to 6). Also, the TLC experiment did not detect product conversion with membranes containing the D90N replacement protein (Fig. 3, lane 4). The kinetic parameters for the transfer reaction with Mg^{2+} and Mn^{2+} showed that replacement of Asp90 and Asp91 had different effects on the enzyme function. In membranes containing the D90E and D90N forms of WecA, the apparent K_m values for Mg^{2+} and Mn^{2+} increased three- to fivefold compared to the apparent K_m of the parental enzyme (Table 3). Also, the ratios of the K_m values for the D90N and D90E forms were 1.2 and 0.6 with Mg^{2+} and Mn^{2+}, respectively (Table 3), indicating that the enzyme affinity for the metal ion did not vary dramatically regardless of the residue charge, which suggests that Asp90 does not interact with either Mg^{2+} or Mn^{2+}. In contrast, in membranes containing the D91N and D91E forms of WecA, the apparent K_m values with Mg^{2+} increased threefold and decreased threefold, respectively, compared to the apparent K_m of the parental enzyme (Table 3). Similar variations were observed with Mn^{2+}. The ratios of the K_m values for the D91N and D91E forms with Mg^{2+} and Mn^{2+} were 11.4 and 6.2, respectively (Table 3), indicating that the D91N substitution resulted in reduced affinity for the metal ions and suggesting that Asp91 interacts with both Mg^{2+} and Mn^{2+}.

The V_{max} values with both metals were more affected for the D90E and D91E forms than for the forms with Asn substitutions, except for a higher-than-wild-type value for the D90N form (Table 3). This suggests that the larger aliphatic chain of glutamic acid at both positions may interfere with enzymatic activity, possibly by altering the geometry of a putative catalytic site.

Topological analysis of WecA demonstrates that Asp90/91 and ASP156 are exposed to the cytosol. The topology of WecA has been predicted only from computer algorithms and was not experimentally assessed. We determined the transmembrane topology of WecA by the substituted cysteine accessibility

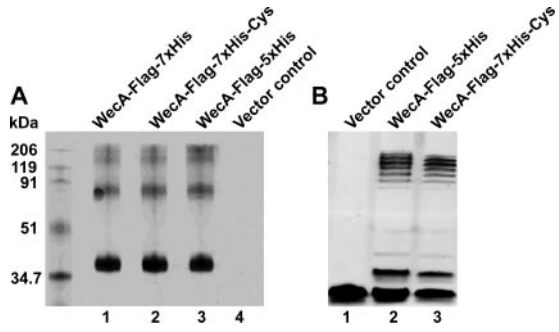

FIG. 6. (A) Expression of $WecA_{FLAG\text{-}7\times His}$. Total membranes were prepared from strain MV501 (VW187 *wecA*::Tn*10*) transformed with various plasmids containing several versions of *wecA* (Table 1). Lane 1, $WecA_{FLAG\text{-}7\times His}$, pJL1; lane 2, $WecA_{FLAG\text{-}7\times His\text{-}Cys}$, cysteineless version of WecA encoded by pJL7; lane 3, $WecA_{FLAG\text{-}5\times His}$, pKV1; lane 4, vector control, pBAD-His. Each lane contained 4 μg of protein. Membranes were transferred to a nitrocellulose membrane and reacted with anti-FLAG monoclonal antibodies. The molecular mass standards were myosin (206 kDa), β-galactosidase (119 kDa), bovine serum albumin (91 kDa), ovalbumin (51 kDa), and carbonic anhydrase (34.7 kDa). (B) Complementation of O7 LPS synthesis in strain MV501 (VW187 *wecA*::Tn*10*). LPS samples were obtained from *E. coli* MV501 (VW187 *wecA*::Tn*10*) transformed with various plasmids. Lane 1, vector control, pBAD-His; lane 2, $WecA_{FLAG\text{-}5\times His}$, pKV1; lane 3, $WecA_{FLAG\text{-}7\times His\text{-}Cys}$, cysteineless version of WecA encoded by pJL7. LPS was separated by Tricine-SDS-PAGE, which was followed by silver staining. Loading was normalized by determining the amount of KDO in the inner core.

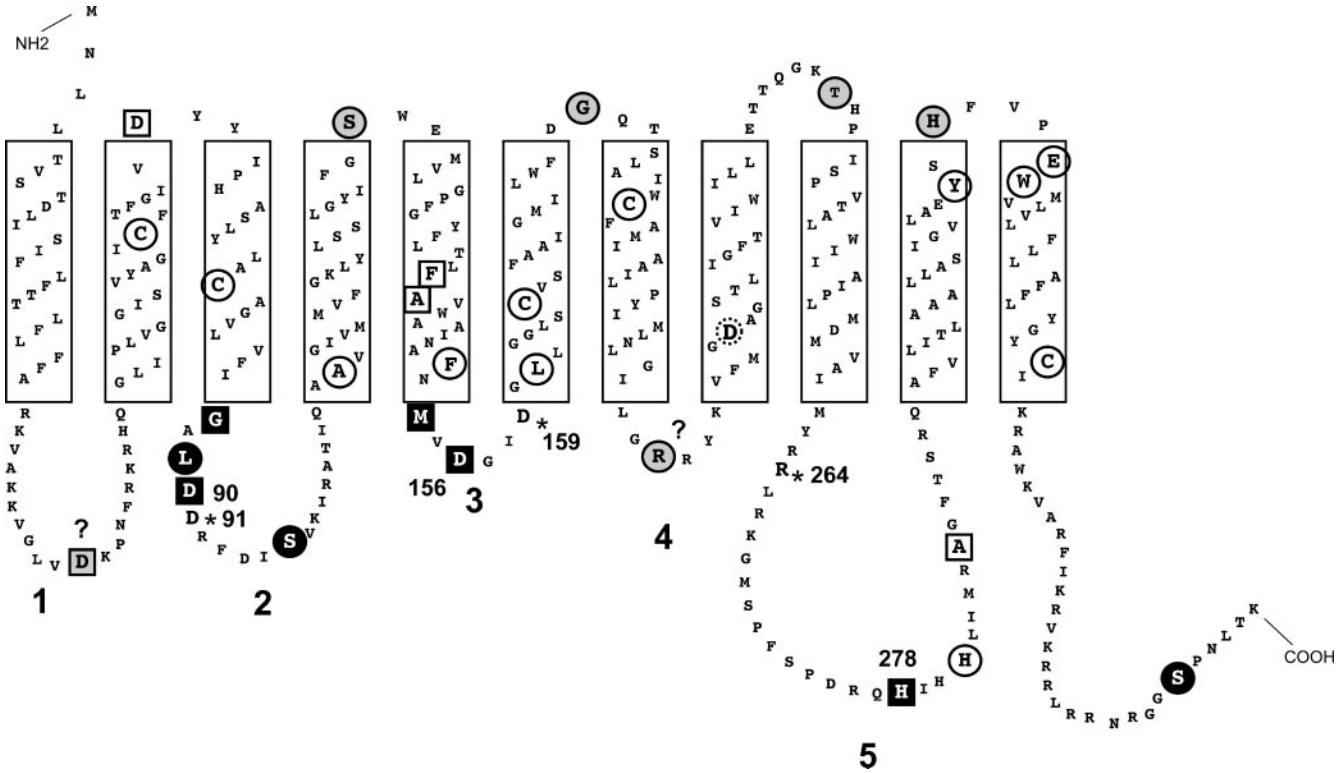

FIG. 7. Topological model of WecA. The model was originally derived by using the TMHHM computer program (49) and was experimentally refined based on the results of the substituted cysteine accessibility experiments (see Fig. 6). Boldface numbers indicate cytosolic loops 1 to 5. The residues spanning predicted transmembrane segments are enclosed in boxes. The individual residues with a gray background are the residues that, when replaced by cysteine, are protected by MTSET from biotin maleimide labeling. The circled residues with a white background are the residues that, when replaced by cysteine, are resistant to labeling by biotin maleimide. The residues with a black background are the residues that, when replaced by cysteine, are labeled with biotin maleimide irrespective of MTSET pretreatment. Squares indicate residues at which cysteine replacement affects the function of WecA, as determined by complementation of O7 LPS synthesis in *E. coli* MV501. Circles indicate residues at which cysteine replacement did not compromise WecA function. The dotted circle indicates Asp217. The asterisks indicate additional residues important for WecA function, which were identified in previous studies (3, 4). The question marks indicate residues where the experimental and predicted topologies do not agree.

method (8). In this method substituted cysteine mutants and a combination of membrane-permeable and membrane-impermeable sulfhydryl-directed chemical labeling reagents are used. WecA contains five cysteine residues located at positions 62, 79, 167, 189, and 337, all of which were replaced by alanine, resulting in cysteineless $WecA_{FLAG\text{-}5\times His}$ (encoded by pJL5 [Table 1]), which was further modified by incorporating two additional histidine residues, resulting in $WecA_{FLAG\text{-}7\times His}$ (encoded by pJL7). The additional histidine residues facilitated WecA binding in Ni^{2+} affinity chromatography (data not shown), a critical step for detection of specific sulfhydryl labeling of this protein. The Cys-to-Ala substitutions and the incorporation of the seven-His tag did not interfere with protein stability or targeting to the plasma membrane (Fig. 6A). Also, the cysteineless WecA forms encoded by pJL5 and pJL7 did not differ in the ability to complement O-antigen LPS production in *E. coli* MV501 compared to the ability of the parental protein encoded by pKV1 (Fig. 6B).

We used pJL7 as a template to construct a library of Cys replacement mutants with mutations at various positions in the WecA protein (Fig. 7). Recombinant plasmids expressing these proteins were transformed into MV501, and each mutant protein was examined by Western blotting to confirm that the Cys replacement did not affect protein stability or targeting to the plasma membrane (Fig. 8). The accessibility of the cysteine residues to the sulfhydryl-reactive reagent biotin maleimide was determined by incubating MV501 with the label, followed by treatment with excess β-mercaptoethanol before lysis. This treatment prevented labeling of any cysteine that became exposed to biotin maleimide during cell fractionation. Biotin maleimide is membrane permeable and can react with thiol groups on either side of the membrane that are next to water molecules since the reaction with an ionized thiol group requires a water molecule as a proton acceptor (8). Therefore, cysteine residues buried in the core of the hydrophobic transmembrane segments are usually not labeled (8). Cys-substituted Asp35, Gly87, Leu89, Asp90, Ser96, Ser128, Met154, Asp156, Gly181, Arg209, Thr239, His278, His316, and Ser362 were accessible to biotin maleimide (Fig. 7 and 8), suggesting they were not located in transmembrane regions (Fig. 7). In contrast, proteins with substitutions in Asp67, Phe143, Ala 106, Ala144, Leu161, His281, Ala287, Tyr314, Glu320, and Tyr321 did not react with the label (Fig. 7 and 8 and data not shown), suggesting that these residues are in close proximity to the inner membrane or are embedded in the membrane bilayer. Cys-substituted Gly87 and Leu89, which were predicted to be in the inner membrane by the computer model (4, 5), were detectable with

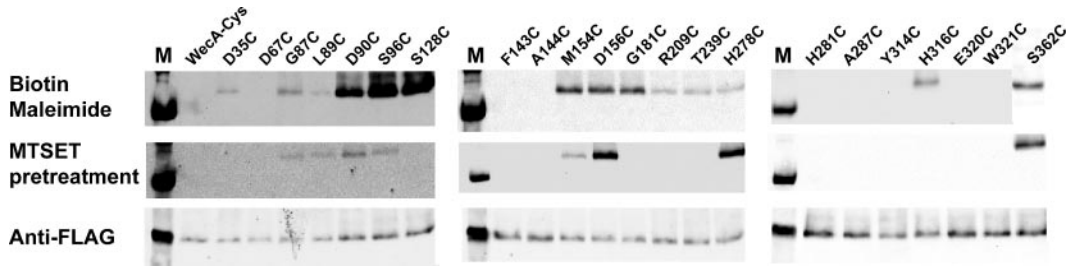

FIG. 8. Sulfhydryl labeling accessibility of cysteine replacements in $WecA_{FLAG\text{-}7\times His}$. The top panel shows the results obtained with biotin maleimide labeling. The middle panel shows the results of biotin maleimide labeling with MTSET-pretreated samples. The lower panel shows Western blots with the FLAG monoclonal antibody. WecA-Cys is the cysteineless WecA protein encoded by pJL7. Each of the replacement mutants is indicated by its short designation (see Fig. 7 for the location of each residue in the topological model of WecA). Biotin maleimide labeling of S362C in the presence and absence of MTSET was done in a different experiment. Lane M contained molecular mass markers.

biotin maleimide. Therefore, we extended the boundaries of cytosolic loop 2 to include these residues (Fig. 7).

To determine the sidedness of the mutated residues in WecA, we used MTSET, a charged thiol-specific probe that reacts with sulfhydryl groups under conditions similar to those used for biotin maleimide but cannot penetrate the cytoplasmic membrane due to its positive charge (8). Incubation of bacterial cells expressing the cysteine-substituted WecA derivatives with MTSET prior to treatment with biotin maleimide prevented labeling of periplasmic cysteine residues. The results of these experiments demonstrated that Cys-substituted Gly87, Leu89, Asp90, Ser96, Met154, Asp156, His278, and Ser362 were labeled by biotin maleimide irrespective of pretreatment with MTSET (Fig. 8), suggesting they were exposed to the cytoplasmic face of the inner membrane. In contrast, labeling of Cys-substituted Ser128, Gly181, Thr239, Tyr314, and His316 did not occur after MTSET pretreatment, suggesting they were exposed to the periplasmic face of the inner membrane. These experiments demonstrated unequivocally that Asp90, Asp91, and Asp156 are exposed to the cytosolic side of the plasma membrane.

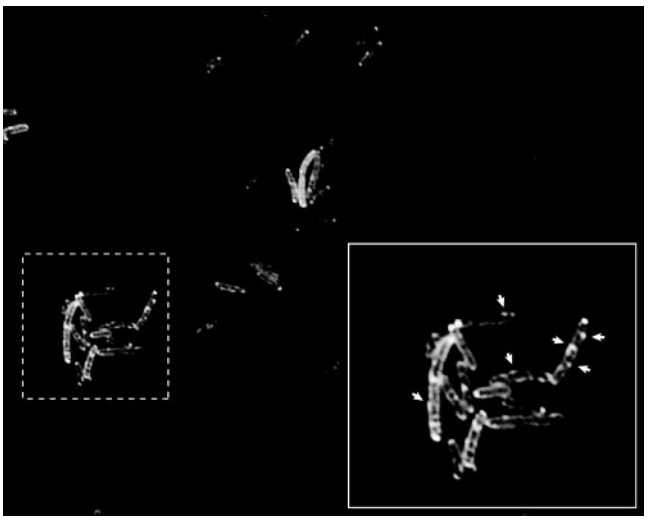

FIG. 9. WecA localizes in discrete membrane domains: fluorescence microscopy of bacteria expressing $WecA_{GFP}$. (Inset) Punctate pattern of fluorescence that is limited to the circumference of bacterial cells. The micrograph was taken with a ×100 oil immersion objective, resulting in a magnification of ×1,000.

The results of cysteine accessibility experiments with the S362C replacement protein suggested that the C-terminal segment of WecA resides in the cytosol. To independently confirm this suggestion, we constructed a C-terminal fusion with GFP, which can fluoresce only if it is present in the cytosol (16). Cells expressing the $WecA_{GFP}$ hybrid displayed fluorescence around the cell perimeter with a punctate pattern (Fig. 9), suggesting that WecA was in the membrane with the C terminus facing the cytosol. The punctate pattern was observed only with bacteria cultured with 0.002% (wt/vol) arabinose in the growth medium. In contrast, when a higher concentration of arabinose (0.2%) was added to the medium, the periphery of the bacterial cells was uniformly fluorescently labeled (data not shown), suggesting that the punctate localization of $WecA_{GFP}$ was not an artifact resulting from protein overexpression. Therefore, we concluded that WecA localized to discrete regions within the membrane.

We also investigated the effects of the Cys-substituted $WecA_{FLAG\text{-}7\times His}$ mutants on O7 antigen expression in vivo using MV501. Replacement of Asp35, Gly87, Asp90, Phe143, Met154, Asp156, and His278 with cysteine precluded complementation of O7 antigen production in MV501. Three of these residues, Asp90, Asp156, and His278, were previously determined to compromise enzyme function (3, 4). Substitution of Asp67, Ala144, and Ala287 partially complemented O7 antigen production, as detected by production of a core band with a single sugar subunit. These results suggested that additional residues, previously not identified, are involved in the WecA function. All the remaining Cys replacements complemented the *wecA* mutation in MV501, as indicated by the formation of a complete O7 polysaccharide (Fig. 10).

DISCUSSION

The detailed mechanism of the transfer reaction of PNPT enzymes is unknown. A double-displacement mechanism has been proposed for MraY, one of the members of this family (18). Double displacement involves the formation of an acyl-phosphoenzyme intermediate due to nucleophilic attack by an active site residue on the sugar nucleotide alpha phosphate, followed by an attack of Und-P that results in

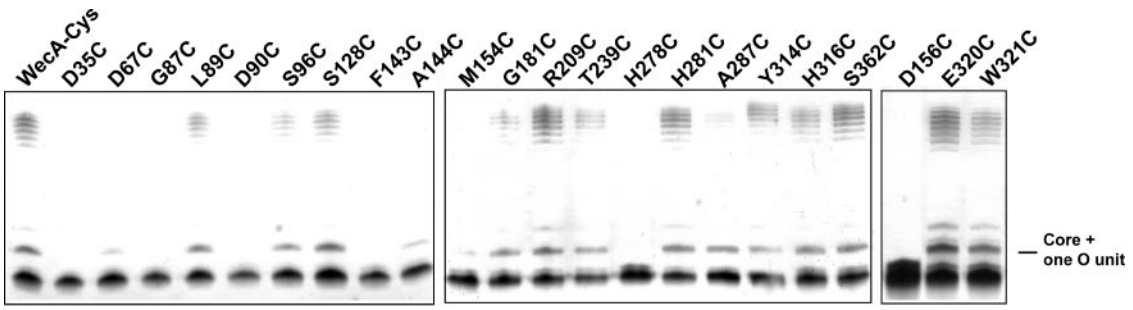

FIG. 10. Complementation of O7 LPS expression in *E. coli* MV501 by plasmids encoding the cysteine-substituted derivatives of cysteineless $WecA_{FLAG\text{-}7\times His}$, as determined with silver-stained polyacrylamide gels. WecA-Cys is the cysteineless WecA protein encoded by pJL7. Each of the replacement mutants is indicated by its short designation (see Fig. 7 for the location of each residue in the topological model of WecA).

displacement of the acyl-enzyme intermediate with transfer of the acyl-1-P residue to Und-P and regeneration of the free enzyme. In this investigation, we examined the functional role of the conserved Asp90, Asp91, Asp156, and Asp159 residues of the *E. coli* WecA protein, a prototypic PNPT that mediates the transfer of the first sugar of the O subunit, GlcNAc, from the nucleotide sugar donor UDP-GlcNAc to the lipid carrier acceptor Und-P. Replacement of Asp156 and Asp159 resulted in a loss of enzyme activity. These two residues are part of a conserved NXXNXXDG IDGL motif in predicted cytosolic loop 3 of the bacterial members of the family (4, 42). We obtained experimental evidence that at least two residues of this motif, Met154 and Asp156, are located on the cytosolic side of the membrane, since when they are replaced by cysteine, they are accessible to biotin maleimide labeling and not protected by pretreatment with MTSET. Also, the M154C replacement resulted in loss of function, as detected by the lack of complementation of O7 LPS production in MV501 cells expressing the $WecA_{FLAG\text{-}7\times His}$ M154C protein, suggesting that this region is important for enzymatic activity.

In a previous study, Asp267 of the *E. coli* MraY protein was proposed to be the active site nucleophile responsible for cleavage of the pyrophosphate bond of the biphosphate nucleotide sugar substrate (28). Asp217 in *E. coli* WecA, located in transmembrane segment 8 (Fig. 7), was predicted to be comparable to Asp267 in MraY (28, 42), but it is not clear how a residue buried in the transmembrane region could access the soluble substrate in the cytosol. In contrast, Asp156 in WecA is clearly exposed to the cytosol, and the kinetic data from the analysis of conservative replacements with Asn and Glu demonstrated that there was a drastic reduction in the enzymatic activity. Moreover, Asp156Glu, Asp156Asn, and Asp156Cys replacements resulted in nonfunctional proteins that could not restore O7 antigen production in MV501. Therefore, our results suggest that the Asp156 residue in WecA may be comparable to the Asp267 residue in MraY, although additional experiments are necessary to demonstrate its involvement in attacking the pyrophosphate bond of UDP-GlcNAc.

The replacement of Asp159 with glutamic acid resulted in a reduced level of catalytic enzyme efficiency. Whereas some bacterial WecA homologues and the eukaryotic members of the family (all of which utilize UDP-GlcNAc as a substrate) have an asparagine in the same location as Asp159 (4), the enzymes with the Asp159Asn replacement also had reduced enzymatic activity compared to that of the parental WecA. Bacteria containing the mutant D159N protein produced dramatically reduced levels of O7 antigen. From these data we concluded that Asp159 may be less critical than Asp156 for the function of WecA. Our results also demonstrate that M154C is defective in O7 antigen synthesis. Therefore, the region in cytosolic loop 3 of WecA spanning at least Met154 through Asp159 plays an important role in enzyme function.

Divalent cations, especially Mn^{2+} and Mg^{2+}, may be involved in the phosphoryl transfer reaction in different enzymes that catalyze the formation of phosphodiester bonds (27). We show here that WecA can function well with either Mg^{2+} or Mn^{2+}, although the kinetic parameters indicated that the enzymatic reaction in vitro is more effective with Mn^{2+}. However, it is likely that either divalent cation may be used in vivo since the optimal concentrations of Mn^{2+} and Mg^{2+} for enzyme activity are below the average concentrations of these metals in bacterial cells, 0.8 mM for Mn^{2+} (2) and 4 mM for Mg^{2+} (29).

In previous studies, a DDXXD motif that is located in predicted cytosolic loop 2 of bacterial PNPTs (this motif corresponds in WecA to $D_{90}DXXD_{94}$) and is also present in the eukaryotic members of the family was proposed to be potentially involved in binding of an Mg^{2+} cofactor (4, 28, 57). This proposal was based on comparisons with prenyl transferases, especially polyprenyl pyrophosphate synthetases (7, 50). These enzymes contain two DDXXD regions that have the carboxylate groups of the aspartic acids, which have been implicated in binding the metal ion, pointing to the active site cleft (50). However, the mechanism of polyprenyl pyrophosphate synthetases is different than the displacement mechanism proposed for PNPTs. Also, PNPTs have only one DDXXD motif. Our data obtained in this study indicate that the $D_{90}DXXD_{94}$ motif in WecA is not analogous to the corresponding motifs in prenyl transferases. First, the kinetic parameters for Mg^{2+} and Mn^{2+} showed that replacement of Asp90 and replacement of Asp91 had different effects on WecA enzyme function. Our results suggest that Asp91, but not Asp90, interacts with either Mg^{2+} or Mn^{2+}. Given that Asp91 is universally conserved in all PNPTs, this residue may be critical for the correct functioning of the enzyme due to its involvement with the metal ion cofactor. Second, we have previously shown that replacement of Asp94 has no effect on WecA function (4), and this residue is much less conserved in the members of the family. Third, we

show here that replacement of Gly87 by cysteine (Fig. 6) destroys enzyme function. Since Gly87 is also highly conserved in PNPTs (4), we propose that the functional motif in these enzymes is $G_{87}XXDD_{91}$, where Asp91 interacts with the metal ion.

Very little information concerning the topology of PNPTs is available. Using β-lactamase fusions, a topological map was constructed for MraY (9), but most of the topological information for other members of the family has been obtained from computer predictions of the transmembrane topology (3, 6, 28, 42). The substituted cysteine accessibility method employed in this study allowed more precise mapping of the boundaries of cytosolic loops 2 and 3 and unequivocal demonstration of the cytosolic location of Asp90, Asp91, and Asp 156. We also demonstrated that His278, a critical residue in cytosolic loop 5 involved in binding of UDP-GlcNAc (3), is indeed exposed to the cytosol. In contrast, other residues in cytosolic loop 5, such as His281 and Ala286, were not accessible to biotinylation when they were replaced by cysteine, suggesting they are in the membrane bilayer or they form part of a structure inaccessible to biotin maleimide. Moreover, when Asp35 and Arg209, located in cytosolic loops 1 and 4, respectively, were replaced by cysteine, the proteins were resistant to biotinylation in the presence of the membrane-impermeable blocking reagent MTSET. The results suggest that these residues are exposed to the periplasmic side of the membrane, which does not agree with the computer predictions. Also, replacement of Asp35 by Cys was associated with loss of complementation of O7 production in strain MV501. We observed in a previous study that replacement of Asp35 by glycine resulted in reduced WecA enzymatic activity and O-antigen production (4). Further analysis is required to define more precisely the boundaries of cytosolic loops 1, 4, and 5 and the function of Asp35. Also, the substituted cysteine accessibility method made it possible to identify additional residues required for WecA function, which were not previously recognized and which are currently being investigated in more detail in our laboratory.

Transferases for the initiation reaction of the O unit and enterobacterial common antigen are the only enzymes in these systems with multiple transmembrane domains, while the other enzymes involved in extension of the glycans are peripheral membrane proteins (43, 52). Fluorescence microscopy with $WecA_{GFP}$ not only confirmed a membrane location but also revealed a punctate distribution rather than a homogenous distribution around the cell perimeter. This observation suggests that WecA may be located in discrete regions within the plasma membrane. Early work with *Salmonella* showed that new O-antigen LPS molecules appear on the cell surface at a limited number of sites (24, 39), and more recent work provided experimental evidence which supports the hypothesis that there are multiprotein complexes for assembly of capsular polysaccharides serving as a molecular "scaffold" across the periplasm (13, 36). Therefore, it is tempting to speculate that other proteins involved in O-antigen assembly, which are thought to interact with each other (31), are also localized in similar membrane domains. Experiments to address this hypothesis are under way in our laboratory.

ACKNOWLEDGMENTS

We thank C. L. Marolda, S. Saldías, B. Henrissat, and C. Creuzenet for critical reading of the manuscript and useful comments.

This study was supported by a grant from the Canadian Institutes of Health Research. M.A.V. holds a Canada Research Chair in Infectious Diseases and Microbial Pathogenesis.

REFERENCES

1. **Alexander, D. C., and M. A. Valvano.** 1994. Role of the *rfe* gene in the biosynthesis of the *Escherichia coli* O7-specific lipopolysaccharide and other O-specific polysaccharides containing *N*-acetylglucosamine. J. Bacteriol. **176:** 7079–7084.
2. **Allingham, J. S., P. A. Pribil, and D. B. Haniford.** 1999. All three residues of the Tn*10* transposase DDE catalytic triad function in divalent metal ion binding. J. Mol. Biol. **289:**1195–1206.
3. **Amer, A. O., and M. A. Valvano.** 2001. Conserved amino acid residues found in a predicted cytosolic domain of WecA (UDP-*N*-acetyl glucosamine:undecaprenol-phosphate *N*-acetylglucosamine-1-phosphate transferase) are implicated in the recognition of UDP-*N*-acetylglucosamine. Microbiology **147:** 3015–3025.
4. **Amer, A. O., and M. A. Valvano.** 2002. Conserved aspartic acids are essential for the enzymic activity of the WecA protein initiating the biosynthesis of O-specific lipopolysaccharide and enterobacterial common antigen in *Escherichia coli*. Microbiology **148:**571–582.
5. **Amer, A. O., and M. A. Valvano.** 2000. The N-terminal region of the *Escherichia coli* WecA (Rfe) protein containing three predicted transmembrane helices is required for function but not for membrane insertion. J. Bacteriol. **182:**498–503.
6. **Anderson, M. S., S. S. Eveland, and N. P. Price.** 2000. Conserved cytoplasmic motifs that distinguish sub-groups of the polyprenol phosphate:*N*-acetylhexosamine-1-phosphate transferase family. FEMS Microbiol. Lett. **191:**169–175.
7. **Ashby, M. N., and P. A. Edwards.** 1990. Elucidation of the deficiency in teo yeast coenzyme Q mutants. Characterization of the structural gene encoding hexaprenyl pyrophospohate synthetase. J. Biol. Chem. **265:**13157–13164.
8. **Bogdanov, M., W. Zhang, J. Xie, and W. Dowhan.** 2005. Transmembrane protein topology mapping by the substituted cysteine accessibility method (SCAM™): application to lipid-specific membrane protein topogenesis. Methods **36:**148–171.
9. **Bouhss, A., D. Mengin-Lecreulx, D. Le Beller, and J. Van Heijenoort.** 1999. Topological analysis of the MraY protein catalysing the first membrane step of peptidoglycan synthesis. Mol. Microbiol. **34:**576–585.
10. **Breton, C., E. Bettler, D. H. Joziasse, R. A. Geremia, and A. Imberty.** 1998. Sequence-function relationships of prokaryotic and eukaryotic galactosyltransferases. J. Biochem. **123:**1000–1009.
11. **Clarke, B. R., D. Bronner, W. J. Keenleyside, W. B. Severn, J. C. Richards, and C. Whitfield.** 1995. Role of Rfe and RfbF in the initiation of biosynthesis of D-galactan I, the lipopolysaccharide O antigen from *Klebsiella pneumoniae* serotype O1. J. Bacteriol. **177:**5411–5418.
12. **Cohen, S. N., A. C. Chang, and L. Hsu.** 1972. Nonchromosomal antibiotic resistance in bacteria: genetic transformation of *Escherichia coli* by R-factor DNA. Proc. Natl. Acad. Sci. USA **69:**2110–2114.
13. **Collins, R. F., K. Beis, B. R. Clarke, R. C. Ford, M. Hulley, J. H. Naismith, and C. Whitfield.** 2006. Periplasmic protein-protein contacts in the inner membrane protein Wzc form a tetrameric complex required for the assembly of *Escherichia coli* group 1 capsules. J. Biol. Chem. **281:**2144–2150.
14. **Dal Nogare, A. R., and M. A. Lehrman.** 1998. Conserved sequences in enzymes of the UDP-GlcNAc/MurNAc family are essential in hamster UDP-GlcNAc:dolichol-P GlcNAc-1-P transferase. Glycobiology **8:**625–632.
15. **Dower, W. J., J. F. Miller, and C. W. Ragsdale.** 1988. High efficiency transformation of *E. coli* by high voltage electroporation. Nucleic Acids Res. **16:**6127–6145.
16. **Feilmeier, B. J., G. Iseminger, D. Schroeder, H. Webber, and G. J. Phillips.** 2000. Green fluorescent protein functions as a reporter for protein localization in *Escherichia coli*. J. Bacteriol. **182:**4068–4076.
17. **Guzman, L. M., D. Belin, M. J. Carson, and J. Beckwith.** 1995. Tight regulation, modulation, and high-level expression by vectors containing the arabinose pBAD promoter. J. Bacteriol. **177:**4121–4130.
18. **Heydanek, M. G., W. G. Struve, and F. C. Neuhaus.** 1969. On the initial stages of peptidoglycan synthesis. III. Kinetics and uncoupling of phospho-N-acetylomuramyl-pentapeptide translocase (uridine 5′-phosphate). Biochemistry **8:**1214–1221.
19. **Higashi, Y., G. Siewert, and J. L. Strominger.** 1970. Biosynthesis of the peptidoglycan of bacterial cell walls. XIX. Isoprenoid alcohol phosphokinase. J. Biol. Chem. **245:**3683–3690.
20. **Kashino, Y.** 2003. Separation methods in the analysis of protein membrane complexes. J. Chromatogr. B Anal. Technol. Biomed. Life Sci. **797:**191–216.
21. **Keenleyside, W. J., and C. Whitfield.** 1996. A novel pathway for O-polysaccharide biosynthesis in *Salmonella enterica* serovar Borreze. J. Biol. Chem. **271:**28581–28592.

22. **Klena, J. D., and C. A. Schnaitman.** 1993. Function of the *rfb* gene cluster and the *rfe* gene in the synthesis of O antigen by *Shigella dysenteriae* 1. Mol. Microbiol. **9:**393–402.
23. **Koonin, E. V., and R. L. Tatusov.** 1994. Computer analysis of bacterial haloacid dehalogenases defines a large superfamily of hydrolases with diverse specificity. Application of an iterative approach to database search. J. Mol. Biol. **244:**125–132.
24. **Kulpa, C. F., Jr., and L. Leive.** 1976. Mode of insertion of lipopolysaccharide into the outer membrane of *Escherichia coli*. J. Bacteriol. **126:**467–477.
25. **Lehrman, M. A.** 1994. A family of UDP-GlcNAc/MurNAc:polyisoprenol-P GlcNAc/MurNAc-1-P transferases. Glycobiology **4:**768–771.
26. **Linton, D., N. Dorrell, P. G. Hitchen, S. Amber, A. V. Karlyshev, H. R. Morris, A. Dell, M. A. Valvano, M. Aebi, and B. W. Wren.** 2005. Functional analysis of the *Campylobacter jejuni N*-linked protein glycosylation pathway. Mol. Microbiol. **55:**1695–1703.
27. **Liu, J., and A. Mushegian.** 2003. Three monophyletic superfamilies account for the majority of the known glycosyltransferases. Protein Sci. **12:**1418–1431.
28. **Lloyd, A. J., P. E. Brandish, A. M. Gilbey, and T. D. Bugg.** 2004. Phospho-*N*-acetyl-muramyl-pentapeptide translocase from *Escherichia coli*: catalytic role of conserved aspartic acid residues. J. Bacteriol. **186:**1747–1757.
29. **Lusk, J. E., R. J. Williams, and E. P. Kennedy.** 1968. Magnesium and the growth of *Escherichia coli*. J. Biol. Chem. **243:**2618–2624.
30. **Marolda, C. L., P. Lahiry, E. Vinés, S. Saldías, and M. A. Valvano.** 2006. Micromethods for the characterization of lipid A-core and O-antigen lipopolysaccharide. Methods Mol. Biol. **347:**237–252.
31. **Marolda, C. L., L. D. Tatar, C. Alaimo, M. Aebi, and M. A. Valvano.** 2006. Interplay of the Wzx translocase and the corresponding polymerase and chain length regulator proteins in the translocation and periplasmic assembly of lipopolysaccharide O antigen. J. Bacteriol. **188:**5124–5135.
32. **Marolda, C. L., J. Welsh, L. Dafoe, and M. A. Valvano.** 1990. Genetic analysis of the O7-polysaccharide biosynthesis region from the *Escherichia coli* O7:K1 strain VW187. J. Bacteriol. **172:**3590–3599.
33. **Marrero, P. F., C. D. Poulter, and P. A. Edwards.** 1992. Effects of site-directed mutagenesis of the highly conserved aspartate residues in domain II of farnesyl diphosphate synthase activity. J. Biol. Chem. **267:**21873–21878.
34. **McCarter, J. D., and S. G. Withers.** 1996. Unequivocal identification of Asp-214 as the catalytic nucleophile of *Saccharomyces cerevisiae* α-glucosidase using 5-fluoro glycosyl fluorides. J. Biol. Chem. **271:**6889–6894.
35. **McGrath, B. C., and M. J. Osborn.** 1991. Localization of the terminal steps of O-antigen synthesis in *Salmonella typhimurium*. J. Bacteriol. **173:**649–654.
36. **McNulty, C., J. Thompson, B. Barrett, L. Lord, C. Andersen, and I. S. Roberts.** 2006. The cell surface expression of group 2 capsular polysaccharides in *Escherichia coli*: the role of KpsD, RhsA and a multi-protein complex at the pole of the cell. Mol. Microbiol. **59:**907–922.
37. **Meier-Dieter, U., K. Barr, R. Starman, L. Hatch, and P. D. Rick.** 1992. Nucleotide sequence of the *Escherichia coli rfe* gene involved in the synthesis of enterobacterial common antigen. Molecular cloning of the *rfe-rff* gene cluster. J. Biol. Chem. **267:**746–753.
38. **Meier-Dieter, U., R. Starman, K. Barr, H. Mayer, and P. D. Rick.** 1990. Biosynthesis of enterobacterial common antigen in *Escherichia coli*. J. Biol. Chem. **265:**13490–13497.
39. **Muhlradt, P. F., J. Menzel, J. R. Golecki, and V. Speth.** 1973. Outer membrane of *Salmonella*. Sites of export of newly synthesised lipopolysaccharide on the bacterial surface. Eur. J. Biochem. **35:**471–481.
40. **Osborn, M. J.** 1963. Studies in the Gram-negative cell wall. I. Evidence for the role of 2-keto-3-deoxyoctonoate in the lipopolysaccharide of *Salmonella typhimurium*. Proc. Natl. Acad. Sci. USA **50:**499–506.
41. **Pedersen, L. B., E. R. Angert, and P. Setlow.** 1999. Septal localization of penicillin-binding protein 1 in *Bacillus subtilis*. J. Bacteriol. **181:**3201–3211.
42. **Price, N. P., and F. A. Momany.** 2005. Modeling bacterial UDP-HexNAc: polyprenol-P HexNAc-1-P transferases. Glycobiology **15:**29R–42R.
43. **Raetz, C. R. H., and C. Whitfield.** 2002. Lipopolysaccharide endotoxins. Annu. Rev. Biochem. **71:**635–700.
44. **Reeves, P. R., M. Hobbs, M. A. Valvano, M. Skurnik, C. Whitfield, D. Coplin, N. Kido, J. Klena, D. Maskell, C. R. H. Raetz, and P. D. Rick.** 1996. Bacterial polysaccharide synthesis and gene nomenclature. Trends Microbiol. **4:**495–503.
45. **Rick, P. D., G. L. Hubbard, and K. Barr.** 1994. Role of the *rfe* gene in the synthesis of the O8 antigen in *Escherichia coli* K-12. J. Bacteriol. **176:**2877–2884.
46. **Rush, J. S., P. D. Rick, and C. J. Waechter.** 1997. Polyisoprenyl phosphate specificity of UDP-GlcNAc:undecaprenyl phosphate N-acetylglucosaminyl 1-P transferase from *E. coli*. Glycobiology **7:**315–322.
47. **Samland, A. K., T. Etezady-Esfarjani, N. Amrhein, and P. Macheroux.** 2001. Asparagine 23 and aspartate 305 are essential residues in the active site of UDP-*N*-acetylglucosamine enolpyruvyl transferase from *Enterobacter cloacae*. Biochemistry **40:**1550–1559.
48. **Samuel, S., and P. Reeves.** 2003. Biosynthesis of O-antigens: genes and pathways involved in nucleotide sugar precursor synthesis and O-antigen assembly. Carbohydr. Res. **338:**2503–2519.
49. **Sonnhammer, E. L. L., G. von Heijne, and A. Krogh.** 1998. A hidden Markov model for predicting transmembrane helices in protein sequences, p. 175–182. *In* J. Glasgow, T. Littlejohn, F. Major, R. Lathrop, D. Sankoff, and C. Sensen (ed.), Proceedings of Sixth International Conference on Intelligent Systems for Molecular Biology. AAAI Press, Menlo Park, CA.
50. **Tarshis, L. C., M. Yan, C. D. Poulter, and J. C. Sacchettini.** 1994. Crystal structure of recombinant farnesyl diphosphate synthase at 2.6-Å resolution. Biochemistry **33:**10871–10877.
51. **Valdivia, R. H., A. E. Hromockyj, D. Monack, L. Ramakrishnan, and S. Falkow.** 1996. Applications for green fluorescent protein (GFP) in the study of host-pathogen interactions. Gene **173:**47–52.
52. **Valvano, M. A.** 2003. Export of O-specific lipopolysaccharide. Front. Biosci. **8:**s452–471.
53. **Valvano, M. A., and J. H. Crosa.** 1989. Molecular cloning and expression in *Escherichia coli* K-12 of chromosomal genes determining the O7 lipopolysaccharide antigen of a human invasive strain of *E. coli* O7:K1. Infect. Immun. **57:**937–943.
54. **Wang, L., D. Liu, and P. R. Reeves.** 1996. C-terminal half of *Salmonella enterica* WbaP (RfbP) is the galactosyl-1-phosphate transferase domain catalyzing the first step of O-antigen synthesis. J. Bacteriol. **178:**2598–2604.
55. **Wang, L., and P. R. Reeves.** 1998. Organization of the *Escherichia coli* O157 O antigen cluster and identification of its specific genes. Infect. Immun. **66:**3545–3551.
56. **Whitfield, C., and M. A. Valvano.** 1993. Biosynthesis and expression of cell-surface polysaccharides in gram-negative bacteria. Adv. Microb. Physiol. **35:**135–246.
57. **Xu, L., M. Appell, S. Kennedy, F. A. Momany, and N. P. Price.** 2004. Conformational analysis of chirally deuterated tunicamycin as an active site probe of UDP-N-acetylhexosamine:polyprenol-P N-acetylhexosamine-1-P translocases. Biochemistry **43:**13248–13255.
58. **Yao, Z., and M. A. Valvano.** 1994. Genetic analysis of the O-specific lipopolysaccharide biosynthesis region (*rfb*) of *Escherichia coli* K-12 W3110: identification of genes that confer group 6 specificity to *Shigella flexneri* serotypes Y and 4a. J. Bacteriol. **176:**4133–4143.
59. **Zhou, T., and B. P. Rosen.** 1999. Asp^{45} is a Mg^{2+} ligand in the ArsA ATPase. J. Biol. Chem. **274:**13854–13858.